

Effects of Postannealing Process on the Properties of RuO₂ Films and Their Performance As Electrodes in Organic Thin Film Transistors or Solar Cells

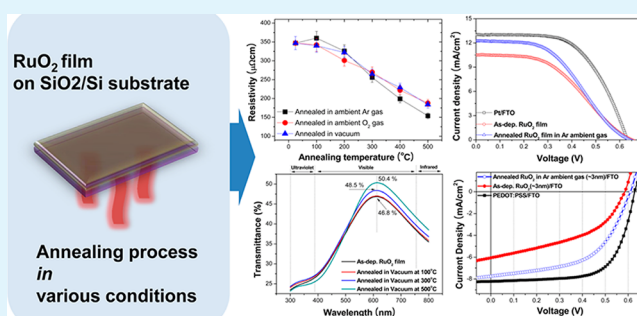
Dong-Jin Yun,^{*,†} Hye-min Ra,[‡] Sae Byeok Jo,[‡] Wanjoo Maeng,[†] Seung-hyup Lee,[†] Sunghoon Park,[†] Ji-Wook Jang,[‡] Kilwon Cho,[‡] and Shi-Woo Rhee^{*,‡}

[†]Samsung Advanced Institute of Technology, Suwon 440-600, Republic of Korea

[‡]Department of Chemical Engineering of Pohang University of Science and Technology (POSTECH), Pohang 790-784, Republic of Korea

ABSTRACT: RuO₂ films were deposited on SiO₂ (300 nm)/N++Si substrates using radio frequency magnetron sputtering at room temperature. As-deposited RuO₂ films were annealed at different temperatures (100, 300, and 500 °C) and ambients (Ar, O₂ and vacuum), and the resulting effects on the electrical and physical properties of RuO₂ films were characterized. The effect of annealing atmosphere was negligible, however the temperature highly influenced the resistivity and crystallinity of RuO₂ films. RuO₂ films annealed at high temperature exhibited lower resistivity and higher crystallinity than as-deposited RuO₂. To investigate the possibility to use RuO₂ film as alternative electrodes in flexible devices, as-deposited and annealed RuO₂ films were applied as the source/drain (S/D) electrodes in organic thin film transistor (OTFT), catalytic electrodes in dye sensitized solar cell (DSSC) and as the hole-injection buffer layer (HIL) in organic photovoltaic (OPV). Except for OTFTs ($\mu \approx 0.45 \text{ cm}^2/(\text{V s})$ and on/off ratio $\approx 5 \times 10^5$) with RuO₂ S/D electrodes, the DSSC and OPV (3.5% and 2.56%) incorporating annealed RuO₂ electrodes showed higher performance than those with as-deposited RuO₂ electrodes (3.0% and 1.61%, respectively).

KEYWORDS: pentacene thin film transistor, annealing process, ruthenium oxide, work-function, dye sensitized solar cell, organic photovoltaic



INTRODUCTION

Ruthenium oxide (RuO₂) is an attractive candidate for source and drain (S/D) electrodes in organic thin film transistors (OTFT) owing to their high work-function ($\sim 5.0 \text{ eV}$).^{1–3} Recently, our group characterized RuO₂ film, which have been mainly used as buffer layers in organic light emitting device (OLED) and silicon devices, as S/D electrodes in OTFTs, and the corresponding devices exhibited higher performance than those using gold (Au) S/D electrodes.^{1,2} Nevertheless, the electrical resistivity of RuO₂ film is still relatively high to replace metallic electrode, such as gold, platinum, or copper electrodes in industry.

In general, thermal annealing processes are utilized with the purpose of modifying the surface or bulk properties of thin films. Even though intrinsic material properties are usually retained, the properties of thin films including crystallinity, bonding states and work-function highly depend on their process conditions.^{4–6} Therefore, it is anticipated that thermal treatment of RuO₂ films can be an efficient way to enhance their electrical conductivity.

RuO₂ films have a high potential to be applied in various fields, such as S/D electrodes in OTFT devices because of

the high work-function, conductivity, and catalytic activity.^{2,3,7,8} The hole injection buffer layer (HIL) at the organic semiconductor/cathode electrode interface in organic photovoltaics (OPV) and the catalyst counter electrode (CCE) of dye sensitized solar cells (DSSC) are good examples of RuO₂ applications, because the buffer layer at organic semiconductor/cathode interfaces and CCE of DSSC require high work-function^{9–11} and catalytic activity^{12–14} for prompt electron/hole transport at semiconductor/cathode or electrolyte/cathode interfaces, respectively. However, the applications of RuO₂ films as the buffer layer of OPV or CCE of DSSC have not been studied intensively despite their excellent electrical properties, while the alternative materials for buffer layers in OPV and CCE of DSSC have been needed for years due to high cost, corrosion or stability problems of conventional buffer layer (poly(3,4-ethylene dioxythiophene)/poly(styrene sulfonate), PEDOT:PSS) and CCE (Platinum) of DSSC.

Received: May 28, 2012

Accepted: August 21, 2012

Published: August 21, 2012

In this work, a radio frequency (r.f.) magnetron sputtering system is used to deposit RuO₂ film using a Ru metal target, and the effects of postannealing processes on the properties of RuO₂ films such as resistivity, crystallinity, work-function and bonding states are characterized. On the basis of above results, as-deposited (as-deposited) and annealed RuO₂ films are applied as S/D electrodes in pentacene TFTs, buffer layers on cathode electrode of OPV and CCE of DSSC, and the associated device performances are examined.

EXPERIMENTAL SECTION

RuO₂ films (thickness = 50 nm) were deposited on SiO₂ (300 nm)/N++Si substrates using r.f. magnetron sputtering with a Ru metal target (2 in. diameter, 99.9%), and the gas flow ratio and sputtering power were fixed at (Ar/O₂ = 25: 25) and 50 W, respectively. The base pressure of the deposition chamber was maintained at 2×10^{-5} Torr and the working pressure was 7×10^{-3} Torr. RuO₂ films were annealed using a furnace at different temperatures (100, 300, and 500 °C) and different ambient gas conditions (Ar and O₂ gas at 1 Torr) and in vacuum (<0.01 Torr) each for 1 h.

Pentacene TFTs, DSSCs and OPVs with as-deposited and annealed RuO₂ films were fabricated to characterize and compare the performance of as-deposited and annealed RuO₂ films as S/D electrodes in pentacene TFT, CCE of DSSC, and buffer layer on cathode electrode of OPV, respectively. The detailed experimental procedures, which were applied to the fabrication of pentacene TFTs, DSSCs, and OPV, are summarized in former publications.^{2,3,10,15,16}

The resistivities and morphologies of RuO₂ films were measured with the 4-point probe method (KEITHLEY 2400 sourcemeter) and atomic force measurement (AFM, veeco nanoscope in NCNT). The crystallinity and optical transmittance of RuO₂ films were investigated by X-ray diffraction (XRD, modified Philips-1880 diffractometer) and UV–vis-spectrophotometry. X-ray and ultraviolet photoemission spectroscopy (XPS and UPS, ESCALAB) were used to analyze the bonding states and work-functions of RuO₂ films. The current–voltage (*I*–*V*) characteristics of pentacene TFT and solar cells (DSSC and OPV) were measured at room temperature using an Agilent E5270A precision semiconductor parameter analyzer and solar simulator equipped with

a source meter (Keithley 2400) and a 300 W xenon lamp (AM 1.5, 100 mW/cm²), respectively.

RESULTS AND DISCUSSION

The crystallinity of as-deposited and annealed RuO₂ films, were characterized by XRD measurement, as shown in Figure 1. The XRD pattern of as-deposited RuO₂ film consists of a (110) main peak, (101), (200), and (211) small peaks, which clearly correspond to RuO₂. After annealing the RuO₂ film, the intensities of the RuO₂ XRD peaks indicating films increase as a function of annealing temperature but there is no significant phase change.^{3,17} On the other hand, RuO₂ films annealed in different atmospheres all result in similar XRD patterns. Thus, it may be deduced that the annealing ambient has negligible effects on the film microstructure and the crystallinity improvement after the annealing process is mainly attributed to the removal of lattice misfits and crystal defects by a thermally assisted mechanism.

Figure 2a shows the AFM images of as-deposited and annealed RuO₂ films. In a way similar to the XRD patterns of annealed RuO₂ films, as annealing temperature increases, the surface

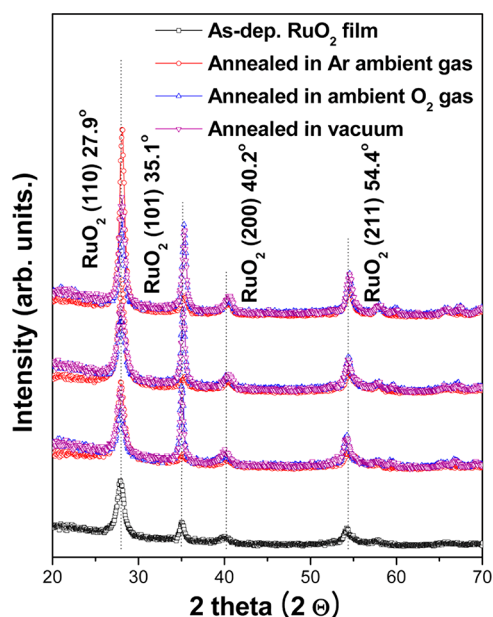


Figure 1. Comparative XRD patterns of as-deposited and annealed RuO₂ films, which were annealed at different temperatures and ambient gas conditions.

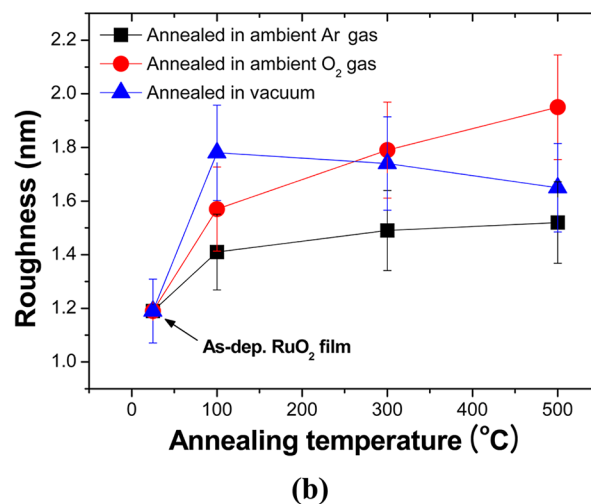
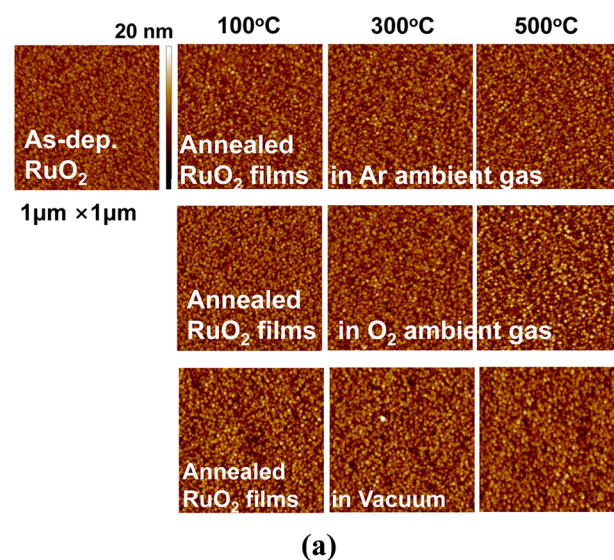


Figure 2. AFM images ($1 \mu\text{m} \times 1 \mu\text{m}$) of as-deposited and annealed RuO₂ films and surface roughness change of RuO₂ films as a function of annealing temperature.

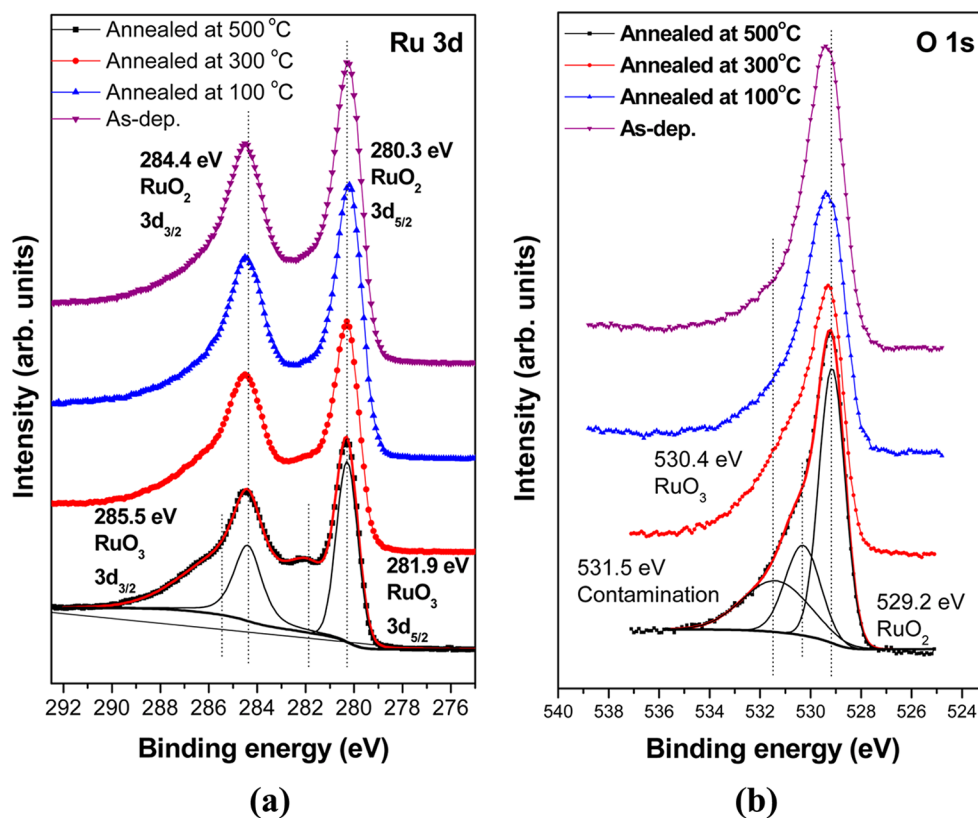


Figure 3. Comparative (a) Ru 3d and (b) O 1s core levels of as-deposited and annealed RuO₂ films in O₂ ambient gas at various annealing temperatures (100, 300, and 500 °C).

roughness and grain size of RuO₂ films slightly increase (<1 nm) but the annealing ambient has no significant effect on the morphology, as summarized in Figure 2b.

The Ru 3d and O 1s core-levels of as-deposited and annealed RuO₂ films were investigated by XPS measurement, as shown in Figure 3a and b. On the basis of the XPS spectra of Ru 3d and O 1s core levels, the annealing temperature and ambient gas condition of annealing process has little effect on the bonding states of RuO₂ films. The Ru 3d and O 1s XPS spectra of as-deposited and annealed RuO₂ films mainly consist of the RuO₂ peaks (Ru 3d_{3/2}, 284.4 eV; Ru 3d_{5/2}, 280.3 eV; O 1s, 529.2 eV), and their relative intensities is preserved even after the annealing process.^{2,17} Compared to the RuO₂ films annealed in Ar gas and vacuum, the RuO₂ films annealed in O₂ atmosphere exhibit the RuO₃ bonding state and the peaks such a state become more intense as the annealing temperature increases. It seems that the formation of RuO₃ bonding originates from the diffusion of highly reactive oxygen gas into RuO₂ film at high temperature.^{18,19}

The resistivity and transmittance changes of RuO₂ films as a function of annealing temperature are shown in Figure 4a and b, respectively. As annealing temperature increases, the resistivity values of RuO₂ films gradually decreased. Independent of ambient gas condition, the RuO₂ films annealed at 100 °C have similar resistivity values near 350 ± 20 μΩcm, which are not distinguished from the resistivity of as-deposited RuO₂ film (347 ± 17 μΩcm). However, the resistivities of RuO₂ films annealed at above 200 °C are lower than those of as-deposited RuO₂ films and further decreased further with increased annealing temperature. Independent of ambient gas condition, the resistivities of RuO₂ films annealed at a fixed annealing temperature

were similar values and the resistivities of RuO₂ films annealed at 300, 400, and 500 °C were approximately 260, 210, and 170 μΩcm, respectively. On the other hand, the transmittance of RuO₂ film was also affected by annealing process in the visible wavelength region as shown in Figure 4b. The transmittance of as-deposited and annealed RuO₂ films (in a vacuum state) are typically compared in Figure 4b, and the transmittance-change of RuO₂ film after annealing was also independent of ambient gas just like other properties such as resistivity, morphology and crystallinity. Both resistivity and transmittance changes may be attributed to crystallinity improvement after the annealing process. It is suspected that the crystallinity improvement reduces light scattering or charge-carrier trapping so that conductivity and transmittance of RuO₂ film could increase.²⁰

UPS measurements of as-deposited and annealed RuO₂ films were performed to analyze the effect of annealing process on the work-function of RuO₂ film. The work-functions of RuO₂ films were calculated using the following eq 1.^{2,3}

$$\phi_M = h\nu (= 21.2 \text{ eV}) - E_{\text{cutoff(metal)}} + E_{\text{Fermi(metal)}} \quad (1)$$

Here, $h\nu$ (=21.2 eV), $E_{\text{cutoff(metal)}}$, and $E_{\text{Fermi(metal)}}$ are incoming photon energy from He I source, secondary cutoff energy of RuO₂ film, and Fermi energy of RuO₂ film, respectively. From eq 1 and the UPS spectra in Figure 5, the work-functions of as-deposited and annealed RuO₂ films were calculated, and as-deposited RuO₂ film showed a work-function value near ~5.2 eV. The work-function of the RuO₂ film slightly decreased after annealing. Regardless of the ambient gas condition (O₂ ambient, Ar ambient or vacuum), the work-functions of RuO₂ films annealed at 300 °C showed 5.17 eV ± 0.05, which are similar values to that of as-deposited RuO₂ film, but the work-functions

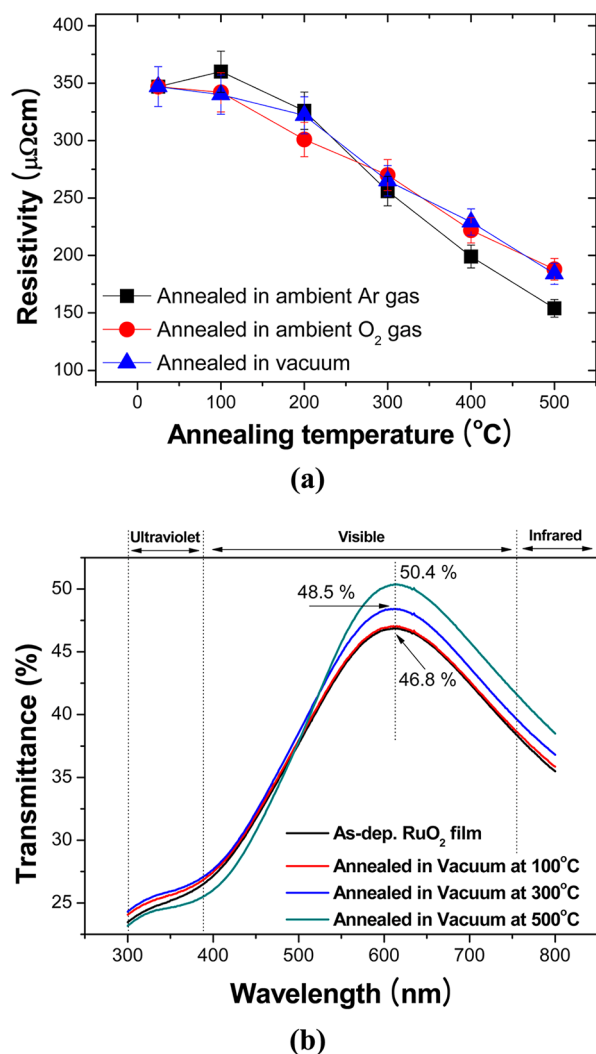


Figure 4. (a) Resistivity and (b) transmittance changes of annealed RuO₂ films in vacuum as a function of annealing temperature.

of RuO₂ film decreased to ~ 5.03 eV after annealing process at 500 $^{\circ}\text{C}$. The work-function change of RuO₂ film is highly related to the crystallinity improvement of RuO₂ film at annealing process. After annealing at high temperature, the crystal defect or lattice misfits at the RuO₂ film surface are suspected to decrease so that the electron density of RuO₂ film at surface region could be increased. As a result, the work-functions of the RuO₂ films slightly decreases after annealing.²⁰

OTFTs, DSSCs, and OPVs with as-deposited and annealed RuO₂ electrodes were fabricated and characterized to investigate the possible use of RuO₂ films as electrodes for organic electronics and the effects of annealing process on the electrode performance.

Bottom-contact pentacene TFTs were fabricated using as-deposited and annealed RuO₂ films as S/D electrodes, as shown Figure 6a. After patterning of the S/D electrodes, annealing was performed and pentacene semiconductor was deposited. The I - V characteristic of the pentacene TFT with as-deposited and annealed RuO₂ S/D electrodes were studied. The field-effect mobility in the saturation regime ($V_D = -40$ V) was calculated using the formula given below:^{2,3}

$$I_{\text{DS}} = \frac{WC_i}{2L}(V_G - V_T)^2 \mu \quad (2)$$

where I_{DS} is the drain current at a specific gate voltage (V_G), W the channel width, L the channel length, V_T the threshold voltage, μ the carrier field effect mobility and C_i the capacitance per unit area of the gate insulator (C_i of 300 nm thick SiO₂ was measured to be 10 nF/cm²). Figure 6 (b) shows the transfer curves of pentacene TFTs with RuO₂ S/D electrodes, which were measured in the backward direction from 20 V to -40 V. The on/off ratio and μ of pentacene TFT were not improved after annealing of the S/D electrodes but the values were comparable to or higher than those of pentacene TFTs with Au S/D electrodes (on/off ratio = 10^6 and $\mu = 0.28$ cm²/(V s)).^{2,3} The μ and on/off ratio of pentacene TFTs with RuO₂ S/D electrode annealed at 300 $^{\circ}\text{C}$ and N₂ ambient gas condition were ~ 0.45 cm²/(V s) and $\sim 5 \times 10^5$, which are almost identical to those of performance with pentacene TFTs with as-deposited RuO₂ S/D electrodes. The pentacene TFT with RuO₂ S/D electrode annealed at 300 $^{\circ}\text{C}$ and N₂ ambient gas condition also showed almost the same output curve to that with as-deposited RuO₂ S/D electrode, as shown in Figure 5c. The resistivity-decrease of RuO₂ S/D electrodes after annealing did not significantly affect to the electrical properties of pentacene TFTs because of the short channel length of the pentacene TFT and the sufficient conductivity of as-deposited RuO₂ S/D film. On the other hand, in the case of pentacene TFT with RuO₂ S/D electrodes annealed at 500 $^{\circ}\text{C}$, μ and on/off ratio unexpectedly degraded to ~ 0.2 cm²/(V s) and $\sim 10^5$ and a hysteresis behavior in the transfer characteristics appeared, as shown in Figure 5b and d. We believe that the performance deterioration of pentacene TFTs originated from the thermal damage of OTS monolayers on the dielectrics after the annealing process. The degradation of OTS monolayers on the gate dielectric induces trap sites near the channel region that hinder transfer of hole carriers in the channel.

The resistivity improvement of RuO₂ films after annealing did not affect the performance of S/D electrodes, but highly improved the performance of large-area electrodes in solar cells. Because RuO₂ has high catalytic activity and conductivity, it is expected that RuO₂ film can be utilized as a catalytic counter electrode between the electrolyte and the conductive counter electrode. The performance of DSSCs with RuO₂ CCE (50 nm) were characterized with a solar simulator under one sun illumination. The I - V curves are shown in Figure 7a and the solar cell parameters including short-circuit current density (J_{sc}), open circuit voltage (V_{oc}), fill factor (FF), and efficiency (η) are summarized in Table 1. The DSSC with as-deposited RuO₂ CCE showed J_{sc} of 10.5 mAcm⁻², FF of 43%, and efficiency of 3.0%, and these results confirmed that the potential use of as-deposited RuO₂ film as a CCE of DSSC, even though the performance of DSSC with RuO₂ film is somewhat inferior to that of Pt CCE ($J_{\text{sc}} = 13.0$ mAcm⁻², FF = 0.58, and $\eta = 4.8\%$). The J_{sc} , FF, and efficiency of DSSC with RuO₂ CCE were further improved up to $J_{\text{sc}} = 12.2$ mAcm⁻², FF = 45%, and $\eta = 3.5\%$ because of the high conductivity of RuO₂ CCE annealed at 500 $^{\circ}\text{C}$.

On the other hand, a potential application of RuO₂ film consists of the HIL between P3HT:PCBM active layer and conducting transparent anode is owing to high work-function (~ 5.0 eV) and conductivity of RuO₂. The HIL that has a high work-function has the role of reducing the interface resistance during the hole-extraction process from the active layer to the anode. As studied by UPS analysis, RuO₂ film has a high work-function (~ 5.0 eV) comparable to that of PEDOT:PSS films (4.9–5.0 eV), which are commonly used as a hole injection layer, and moreover the conductivity of RuO₂ film is much higher than

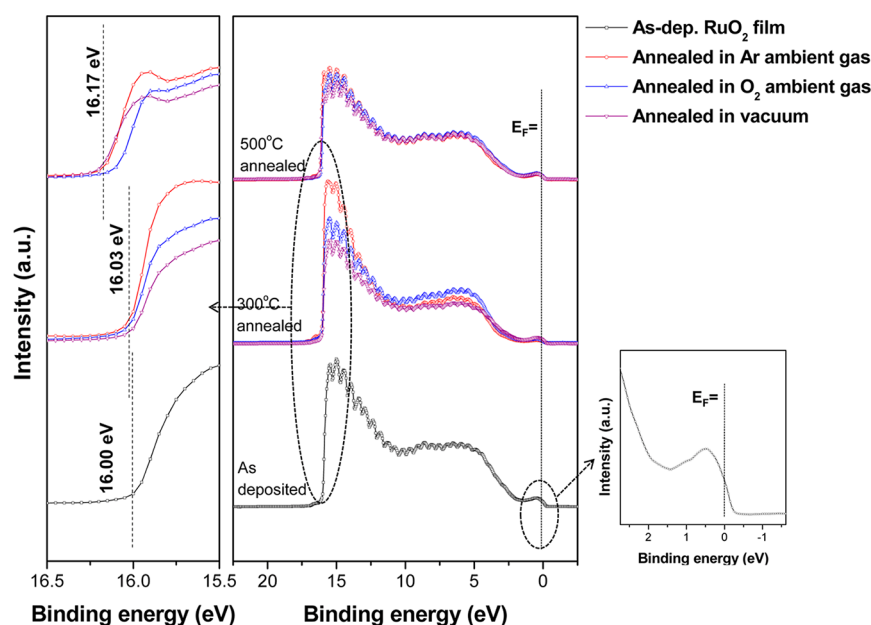


Figure 5. Comparative UPS spectra including Secondary cutoff and Fermi edge regions of as-deposited and annealed RuO₂ films under various conditions.

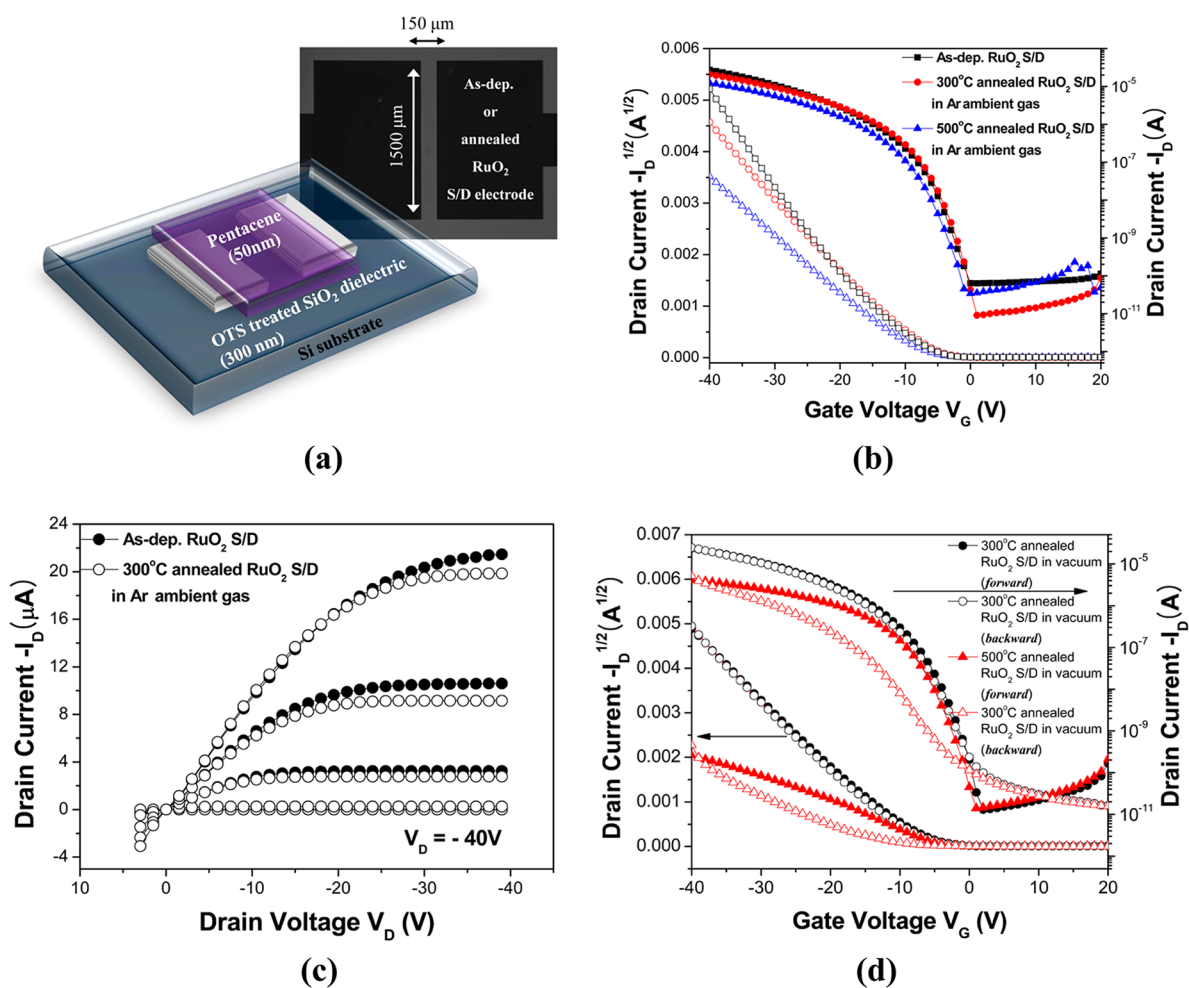


Figure 6. (a) Schematic diagram of a bottom-contact pentacene TFT with S/D electrode, comparative (b) transfer and (c) output characteristics of pentacene TFTs with as-deposited and annealed RuO₂ S/D electrodes, and (d) current–voltage hysteresis of pentacene TFTs with RuO₂ S/D electrodes annealed at 300 and 500 °C.

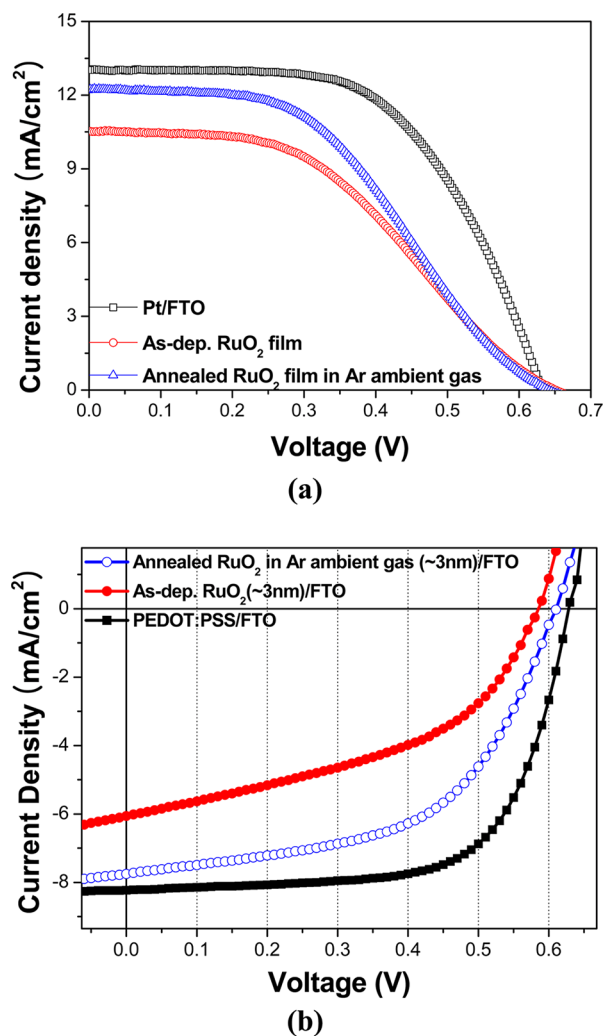


Figure 7. Comparative I – V characteristics of (a) DSSC and (b) OPV with RuO_2 and reference electrodes.

conducting polymers including PEDOT:PSS. The I – V characteristics of OPVs with different buffer layers (PEDOT:PSS and RuO_2 thin films) are shown in Figure 7b. As shown in Figure 6 and Table 1, the photoelectronic conversion efficiency of an OPV cell with as-deposited RuO_2 buffer layer was 1.61%, which value is much poorer than that of OPV with PEDOT:PSS buffer layer (3.45%) because of low J_{sc} (6.06 mA/cm^2). After annealing the RuO_2 buffer layer, the hole transport between active layer and conducting transparent anode was improved owing to the conductivity enhancement of the RuO_2 buffer layer, and thus the J_{sc} (7.75 mA/cm^2) and η (2.56%) of OPV with RuO_2 buffer layer are shown to approach the performance of OPV cells with a PEDOT:PSS buffer layer (J_{sc} : 8.23 mA/cm^2 and η : 3.45%).

CONCLUSIONS

RuO_2 films deposited by r.f. sputtering were annealed at various conditions and the property variations of RuO_2 films depending on annealing condition were clearly characterized. There is no significant effect of ambient gas during the annealing process on the properties of RuO_2 film, but higher annealing temperatures resulted in lower resistivity values. The resistivity reduction after the annealing process did not improve the performance of RuO_2 films as S/D electrodes of organic thin film transistors but highly improved the catalytic performance as an electrode in OPV. Therefore, RuO_2 material is a strong alternative candidate for replacing expensive common electrodes in organic electronics.

AUTHOR INFORMATION

Corresponding Author

*E-mail: DongJin.Yun@samsung.com (D.-J.Y.); Srhee@postech.ac.kr (S.-W.R.). Tel: 82-54-275-2265. Fax: 82-54-2798619.

Notes

The authors declare no competing financial interest.

ACKNOWLEDGMENTS

This research was supported by the Korea Science and Engineering Foundation (KOSEF) through the National Research Laboratory Project, Polymer Gel Cluster group of the Korean government and the Pohang Accelerator Laboratory that provided the synchrotron radiation source at the 4B1 beamlines used in this study. The author D.J.Y. is grateful to Y. K. Lee (researcher at POSTECH) and H. Park (researcher at NCNT) for supporting photolithography and AFM analysis, respectively.

REFERENCES

- (1) Kim, S. W.; Baik, J. M.; Lee, J. L. *Electrochem. Solid-State Lett.* **2005**, *8*, H79.
- (2) Yun, D. J.; Rhee, S. W. *J. Mater. Chem.* **2005**, *20*, 9754.
- (3) Yun, D. J.; Lee, S.; Yong, K.; Rhee, S. W. *Appl. Phys. Lett.* **2010**, *97*, 073303.
- (4) Kim, W. G.; Rhee, S. W. *Microelectron. Eng.* **2009**, *86*, 2153.
- (5) Yun, D. J.; Rhee, S. W. *Org. Electron.* **2008**, *9*, 551.
- (6) Chang, J. F.; Lin, W. C.; Hon, M. H. *Appl. Surf. Sci.* **2001**, *183*, 18.
- (7) Rolison, D. R.; Hagans, P. L.; Swider, K. E.; Long, J. W. *Langmuir* **1999**, *15*, 774.
- (8) Ma, H.; Liu, C.; Liao, J.; Su, Y.; Xue, X.; Xing, W. *J. Mol. Catal. A: Chem.* **2006**, *247*, 7.
- (9) Giroto, C.; Voroshazi, E.; Cheynst, D.; Heremans, P.; Rand, B. P. *ACS Appl. Mater. Interfaces* **2011**, *3*, 3244.
- (10) Kim, J. S.; Park, J. H.; Lee, J. H.; Jo, J.; Kim, D. Y.; Cho, K. *Appl. Phys. Lett.* **2007**, *91*, 112111.
- (11) Choulis, S. A.; Choong, V. E.; Patwardhan, A.; Mathai, M. K.; So, F. *Adv. Func. Mater.* **2006**, *16*, 1075.
- (12) Fang, X.; Ma, T.; Guan, G.; Akiyama, M.; Kida, T.; Abe, E. *J. Electrochem. Soc.* **2004**, *570*, 257.
- (13) Suzuki, K.; Yamaguchi, M.; Kumagai, M.; Yanagida, S. *Chem. Lett.* **2003**, *32*, 28.

Table 1. Photoelectronic Characteristics of DSSC and OPVs with RuO_2 and Reference Electrodes

device type	electrode	V_{OC} (mV)	J_{SC} (mA cm^{-2})	FF (%)	H (%)
DSSC	Pt/FTO	633.1 ± 0.5	13.0 ± 0.2	58 ± 0.5	4.8 ± 0.5
	as-deposited RuO_2 (50 nm)/FTO	651.2 ± 0.5	10.5 ± 0.2	43 ± 0.5	3.0 ± 0.5
	annealed RuO_2 /FTO in Ar ambient gas	639.1 ± 0.5	12.2 ± 0.2	45 ± 0.5	3.5 ± 0.5
OPV	PEDOT:PSS/FTO	630 ± 0.5	8.23 ± 0.2	63 ± 0.2	3.45 ± 0.2
	as-deposited RuO_2 (~ 3 nm)/FTO	590 ± 0.5	6.06 ± 0.2	59 ± 0.2	1.61 ± 0.2
	annealed RuO_2 /FTO in Ar ambient gas	610 ± 0.5	7.75 ± 0.2	61 ± 0.2	2.56 ± 0.2

- (14) Murakami, T. N.; Gratzel, M. *Inorg. Chim. Acta* **2008**, *361*, 572.
- (15) Ganapathy, V.; Karunakaran, B.; Rhee, S. W. *J. Power Sources* **2010**, *195*, 5138.
- (16) Jo, S. B.; Lee, J. H.; Sim, M.; Kim, M.; Park, J. H.; Choi, Y. S.; Kim, Y.; Ihn, S. G.; Cho, K. *Adv. Funct. Mater.* **2011**, *1*, 690.
- (17) Lee, D. J.; Kang, S. W.; Rhee, S. W. *Thin Solid Films* **2002**, *413*, 237.
- (18) Subhramannia, M.; Balan, B. K.; Sathe, B. R.; Mulla, I. S.; Pillai, V. K. *J. Phys. Chem. C* **2007**, *111*, 16593.
- (19) Kim, Y. J.; Gao, Y.; Chambers, S. A. *Appl. Surf. Sci.* **1997**, *120*, 250.
- (20) Vayunandana Reddy, Y. K.; Mergel, D. *J. Mater. Sci.* **2006**, *17*, 1029.